Fully Printed Memristors Made with MoS_2 and Graphene Water-Based Inks

Zixing Peng,[1] Alessandro Grillo,[1] Aniello Pelella,[2] Xuzhao Liu,[3,4] Matthew Boyes,[1] Xiaoyu Xiao,[5] Minghao Zhao,[1] Jingjing Wang,[1] Zhirun Hu[5], Antonio Di Bartolomeo,[2] Cinzia Casiraghi[1]*

[1]Department of Chemistry, University of Manchester, Oxford Road, Manchester, UK

[2]Physics Department "E. R. Caianiello", University of Salerno, via Giovanni Paolo II n. 132, Fisciano, Salerno, Italy

[3]Department of Materials, University of Manchester, Oxford Road, Manchester, UK

[4]Photon Science Institute, University of Manchester, Oxford Road, Manchester, UK

[5]Department of Electrical and Electronics, University of Manchester, Oxford Road, Manchester, UK

Content

S1. State of Art on printed 2DM-based memristors

Supplementary Table I. State of art of Memristors fabricated by solution-based materials using the printing method on rigid substrates.

Structure(thickness); substrate	solvent/additives	Printing technique	Ratio	Set/Reset voltage	Ref
Ag/MoS_2(650 nm)/Gr; SiO_2/Si substrate	Water based solvent	Inkjet printing	10^3-10^5	Set 2V; Reset 0.24 V	Our work
Ag/ZnO(310 nm)/Ag; Glass substrate	Ethanol	Electrohydrodynamic printing, spin coating	10^1	Set 2 V; Reset -2 V	[1]
Ag/ZnO(140 nm)/Cu; SiO_2/Si substrate	Ethanol mixed with Triton X-100	Electrohydrodynamic Printing	10^3	Set 1.25 V; Reset -1.25 V	[2]
Ag/TiO_2(110 nm)/Cu; SiO_2/Si substrate	PVP (0.01 g/ml) in Ethanol	Electrohydrodynamic Printing	10^2	Set 0.7 V; Reset -0.7 V	[3]
Ag/$ZnSnO_3$(190 nm)/Ag; Glass substrate	Triton, acetone, and ethanol	Screen Printing, Electro-hydrodynamic Atomization	10^1	Set 2 V; Reset -2 V	[4]
Au/Cu-SiO_2 NWs(4.5 um)/Cu; Glass/polyimide substrate	MeOH, 1.5wt% ethylcellulose and 10% a-terpineol	Aerosol-Jet Printing	10^5	Set 3 V; Reset -3 V	[5]
Ag/a-TiO_2(80-350 nm)/Ag; Glass substrate	Propylene glycol methylether and ethylene glycol	Inkjet Printing	10^1	Set 10 V; Reset -10 V	[6]
Ag/ZnO(150 nm)/Ag; Glass substrate	ZnO 40% nano-particle colloid solution (Sigma Aldrich)	Electrohydrodynamic Printing	10^3	Set 3.75 V; Reset -3.75 V	[7]
Ag/ZrO_2(120 nm)/Ag; Glass substrate	unknown	Electrospray Deposition, Electrohydrodynamic Printing	10^1	Set 3.8 V; Reset -2.6 V	[8]
Ag/h-BN(250 nm)/Ag; Glass substrate	Water-CMC (carboxy methyl cellulose) solvent.	Inkjet Printing	10^3	Set 2 V; Reset -1 V	[9]

Supplementary Table II(a). State of art of Memristors fabricated by solution-based materials using the printing method on polymer flexible substrates.

Structure(thickness); substrate	solvent/additives	Printing technique	Ratio	Set/Reset voltage	Ref
Ag/MoS_2(650 nm)/Gr; Kapton substrate	Water based solvent	Inkjet printing	10^2-10^3	Set 1V; Reset 0.21 V	Our work
Ag/MoS_2(150 nm)/Ag; Polyimide substrate	IPA and 2-butanol mixture	Aerosol-Jet Printing	10^5-10^7	Set 0.18 V - 0.30 V, Reset -0.1 V	[10]
Ag/WSe_2(300 nm)/Ag; Kapton substrate	Ethanol	Aerosol-Jet Printing, Pneumatic atomizer	10^1-10^2	Set 0.7 V; Reset -0.25 V	[11]
Ag/TiO_2(50-100 um)/Carbon; Paper substrate	Acetyl acetone, DI water, ethanol and ethylene glycol.	Screen Printing, Inkjet Printing	10^1-10^3	Set 1 V; Reset -3 V	[12]
Ag/PVOH-$ZnSnO_3$(250 nm)/Ag; PET substrate	NMP	Reverse Offset Printing, EHD Atomization	10^2	Set 1.5 V; Reset -1.5 V	[13]
Ag/ZrO_2(680 nm)/Ag; Polyimide substrate	unknown	Electrohydrodynamic Printing	10^2	Set 3 V; Reset -3 V	[14]
Ag/Cr-N-doped TiO_2/Ag; PET substrate	unknown	Reverse offset printing EHD Printing EHDA Printing	10^3	Set 1 V; Reset -1 V	[15]

Supplementary Table II(b). State of art on the bendability test reported for memristors fabricated with solution-processed nanomaterials.

Structure; substrate	Cycle endurance	Bending endurance	Bending radius (Minimum)	Ref
Ag/MoS_2/Gr; Kapton substrate	100 cycles	500 times	1.25 mm (2% strain)	Our work
Ag/MoS_2/Ag; Polyimide substrate	100 cycles	1000 times	5 cm	[10]
Ag/WSe_2/Ag; Kapton substrate	unknown	unknown	5 cm	[11]
Ag/TiO_2/Carbon; Paper substrate	100 cycles	1000 times	10 mm	[12]
Ag/PVOH-$ZnSnO_3$/Ag; PET substrate	500 cycles	1500 times	10 mm	[13]
Ag/ZrO_2/Ag; Polyimide substrate	140 cycles	500 times	10 mm	[14]
Ag/Cr-N-doped TiO_2/Ag; PET substrate	500 cycles	100 times	2.5 mm	[15]

S2. Fully printed Ag/MoS_2/Gr memristors on silicon

S2.1 Silver electrode thickness

Devices were made by printing the Ag ink with one and two printing passes (PPs). The corresponding film thickness is shown in **Figure S1 (a)**. **Figure S1 (b)** shows the optical pictures of two representative devices. One can see that an excessively thick Ag electrode might lead to cracks once the dielectric layer is printed on top of it. The cracked device does not show any memristic effect, as shown in **Figure S1 (c)**. Hence, 1 PP was used to print the silver electrodes, corresponding to a thickness of ~ 98 nm and RMS of ~ 53 nm.

Figure S1 (a) Average thickness and RMS for Ag lines vs. printed passes on SiO_2/Si. (b) The optical image of the MoS_2 film print on different print passes of Ag electrode. (c) Typical RS I-V curves of Ag/MoS_2/Gr memristors with different print passes of Ag electrode.

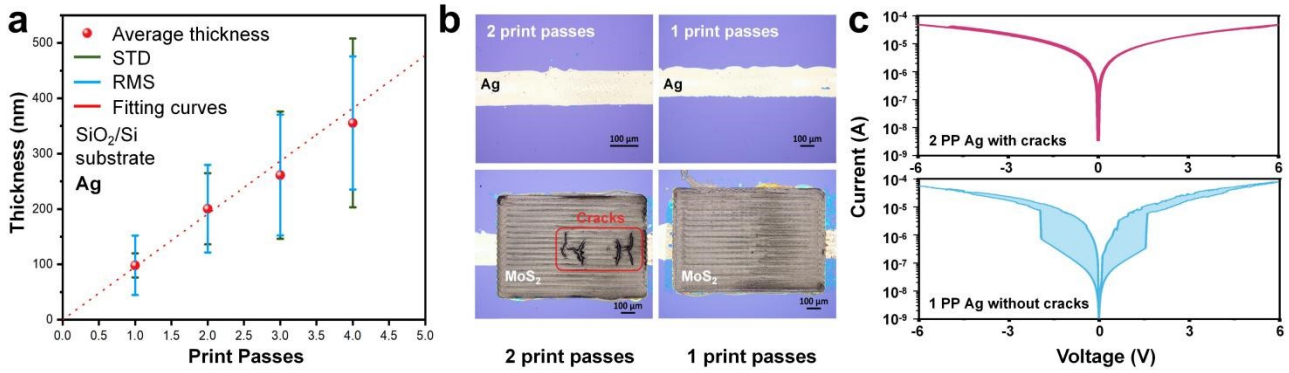

S2.2 Overlapped area

As the memristic effect is expected to be caused by migration of silver ions and formation of conductive filaments, the overlapped area between the silver electrode, the dielectric layer and the top electrode is expected to affect the performance of the device. Hence, we have changed the area by changing the width of the Ag from 0.1 mm to 0.5 mm and investigated if and how the electrical characteristic of the device is affected by this parameter.

The optical images of the devices are shown in **Figure S2**. **Figure S3** show that Ag/MoS_2/Gr memristors achieves higher RS ratio with a relatively small active area. This seems to be counterintuitive, however one should take into account that uniformity of the film is reduced by printing over larger areas, and this may affect the quality of the interface between the electrode and the dielectric layer. Remarkably, the device made with 0.2 mm width Ag bottom electrode and STS annealing shows the best performance, amongst all devices investigated, as shown in **Figure S4**.

Figure S2. Optical images of the Ag/MoS_2/Gr memristor with different bottom Ag electrode widths (0.1 mm- 0.5 mm).

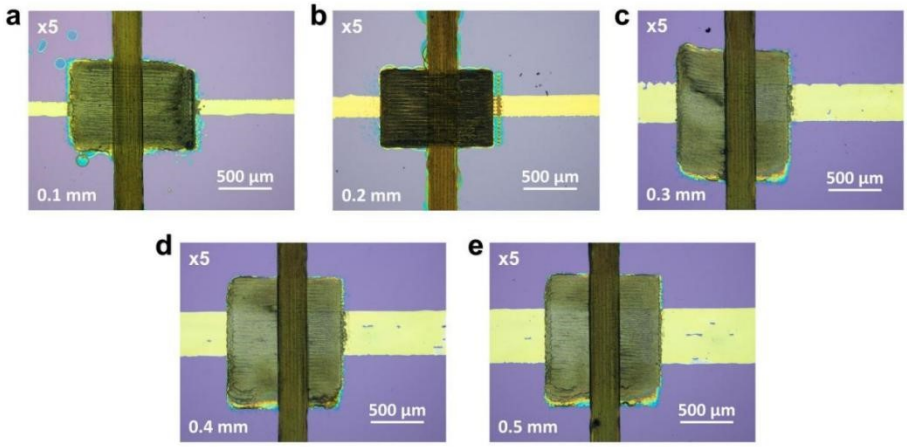

Figure S3. Resistive switching characteristics of STS annealed Ag/MoS_2/Gr memristors, tested over 10 cycles. (a-f) I-V curves for STS annealing Ag/MoS_2/Gr memristors made with different bottom Ag electrode widths: (a) 0.1 mm; (b) 0.2 mm; (c) 0.3 mm; (d) 0.4 mm; (e) 0.5 mm.

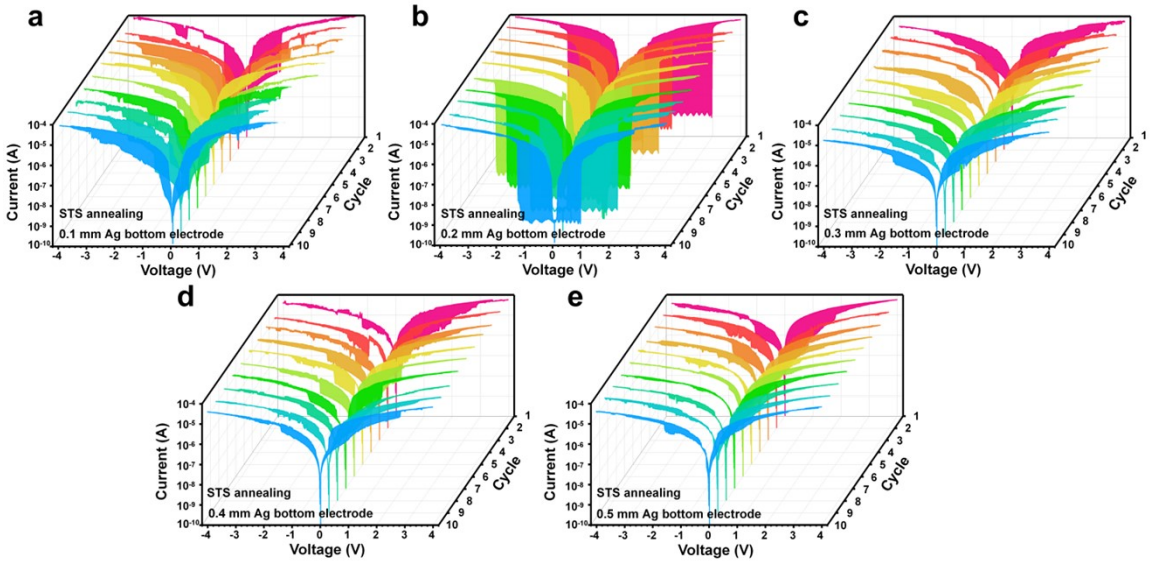

Figure S4. Performance of devices made with bottom electrode width ranging from 0.1 to 0.5 mm and STS annealing.

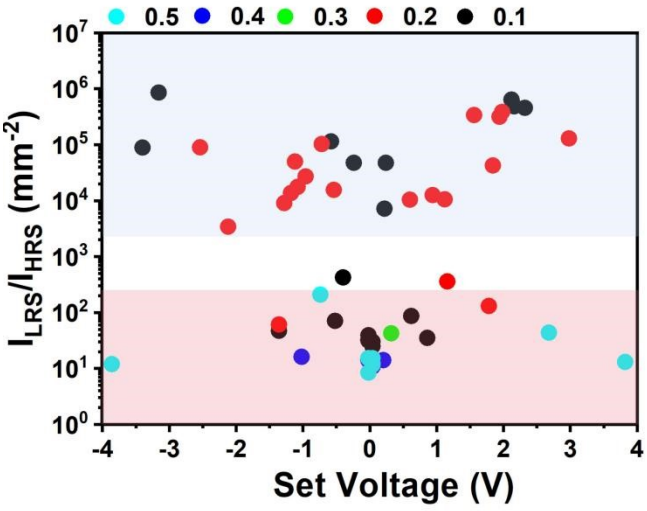

S3. Summary of all devices printed on silicon

Figure S5. (a) I-V curves over 10 cycles of the device made with FS annealing (b) Area normalized (by mm^{-2}) RS ratio for over 100 devices made by STS and FS annealing under different geometries.

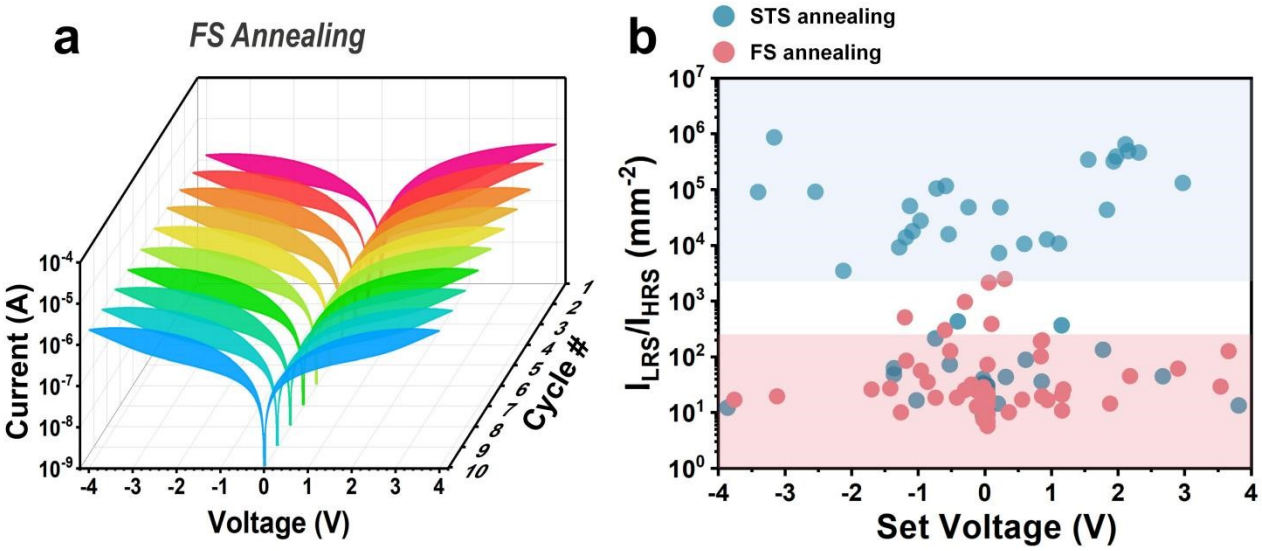

Supplementary Table III. Summary of Ag/MoS_2/Gr tested and their fabrication processing.

Number of samples	Annealing	Ag Thickness & width	Gr Thickness & width	MoS_2 Thickness & length × width
2	STS	2 PP (~100 nm); 0.2 mm	60 PP (~200 nm); 0.2 mm	80 PP(~650 nm); 1.0 mm × 0.6 mm
10	STS	1 PP (~100 nm); 0.1 mm	60 PP (~200 nm); 0.2 mm	80 PP(~650 nm); 1.0 mm × 0.6 mm
10	STS	1 PP (~100 nm); 0.2 mm	60 PP (~200 nm); 0.2 mm	80 PP(~650 nm); 1.0 mm × 0.6 mm
10	STS	1 PP (~100 nm); 0.3 mm	60 PP (~200 nm); 0.2 mm	80 PP(~650 nm); 1.0 mm × 0.8 mm
10	STS	1 PP (~100 nm); 0.4 mm	60 PP (~200 nm); 0.2 mm	80 PP(~650 nm); 1.0 mm × 0.8 mm
10	STS	1 PP (~100 nm); 0.5 mm	60 PP (~200 nm); 0.2 mm	80 PP(~650 nm); 1.0 mm × 1.0 mm
10	FS	1 PP (~100 nm); 0.1 mm	60 PP (~200 nm); 0.2 mm	80 PP(~650 nm); 1.0 mm × 0.6 mm
10	FS	1 PP (~100 nm); 0.2 mm	60 PP (~200 nm); 0.2 mm	80 PP(~650 nm); 1.0 mm × 0.6 mm
10	FS	1 PP (~100 nm); 0.3 mm	60 PP (~200 nm); 0.2 mm	80 PP(~650 nm); 1.0 mm × 0.8 mm
10	FS	1 PP (~100 nm); 0.4 mm	60 PP (~200 nm); 0.2 mm	80 PP(~650 nm); 1.0 mm × 0.8 mm
10	FS	1 PP (~100 nm); 0.5 mm	60 PP (~200 nm); 0.2 mm	80 PP(~650 nm); 1.0 mm × 1.0 mm

S4 Films characterization

Note that because of the large thickness and high roughness, characterization of the arrangement of the nanosheets and their interfaces is extremely challenging with traditional techniques.

We have performed profilometry of the individual printed films before and after annealing (**Figure S6**), but all variations are within experimental errors, so no changes are observed. We have also performed cross sectional SEM measurements (**Figure S7**), but the resolution of the SEM is not high enough to clearly see any difference in the quality of the interfaces or in the arrangement of the nanosheets. The thickness extracted from the SEM pictures is in good agreement with the one obtained by profilometry. For example, in **Figure S7**, the MoS_2 thickness is around 520 nm, in agreement with profilometry, which for 80 printing passes gives a thickness of 672±303 nm; the graphene thickness is around 170 nm, in agreement with profilometry, which for 60 printing passes gives a thickness of 164±102 nm. Finally, the Ag thickness is around 60 nm, in agreement with profilometry, which gives a thickness of 98±53 nm for 1 printing pass.

Figure S6. Average thickness and standard deviation, as measured from the RMS roughness, of the silver, MoS_2 and graphene films, before and after annealing 150 °C for 180 min.

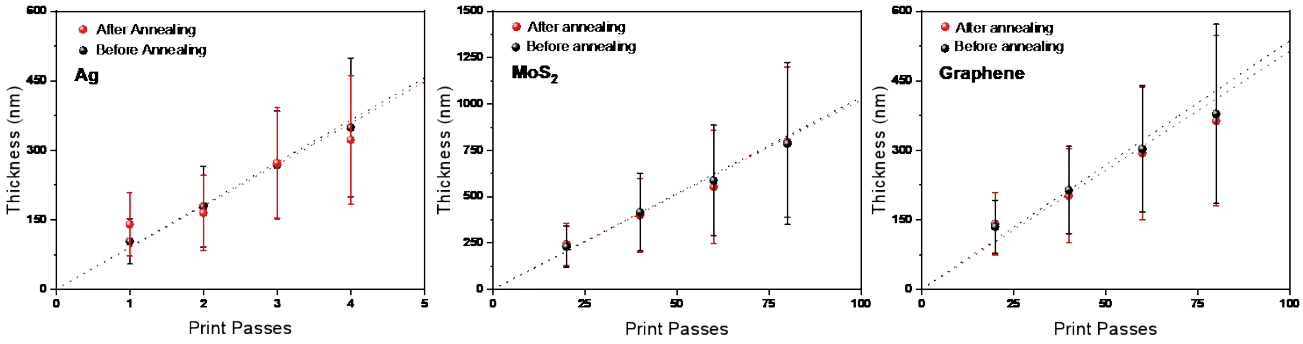

Figure S7. Cross sectional SEM measurement of a STS Ag/MoS_2/Gr memristor.

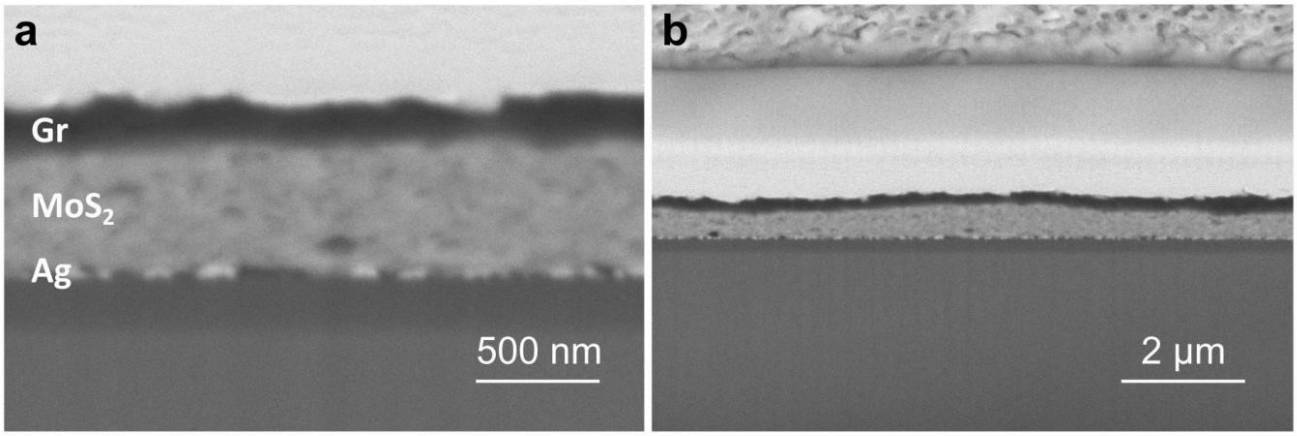

Figure S8. XRD spectra of annealed MoS_2 and pristine MoS_2 film drop-casted on SiO_2/Si substrate, as compared to the reference: PDF #65-1951.

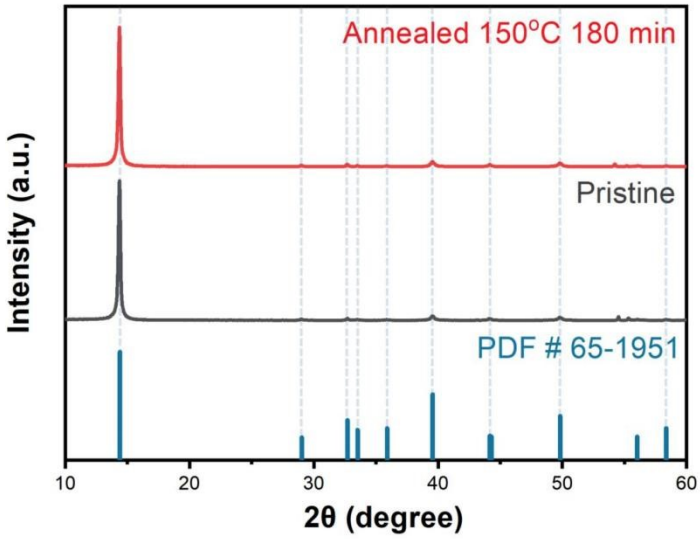

Figure S8 shows an X-ray diffraction (XRD) scan of the annealed and pristine MoS_2 films drop-cast on SiO_2/Si substrate. The peaks are indexed to the lattice planes of hexagonal MoS_2 according to the comparison with the reference (PDF card #65-1951, P63/mmc, a=3.160 Å,c=12.294 Å) for both samples. There is no other new phase introduced into the MoS_2 films.[16]

Figure S9 shows the XPS spectra for Mo 3d and S 2p obtained from both annealed MoS_2 and pristine samples. The most prominent Mo 3d and S 2p doublets in both samples were observed at binding energy values of 229.6 eV (corresponding to Mo^{4+} $3d_{5/2}$) and 162.5 eV (S $2p_{3/2}$), consistent with previous works.[17] Notably, we also detected smaller doublets at lower binding energies (235.9 eV) in the Mo 3d spectra, indicative of the presence of nonstoichiometric Mo^{6+}. This occurrence might be attributed to the presence of MoO_3 produced from the ink preparation.[17]

To study the impact of annealing on the MoS_2 film, we looked at changes in the PS1 content before and after the annealing process. In **Figure S9 b and f**, we analyzed the smaller peaks at higher binding energy in the S 2p spectra, revealing doublets with binding energy values at 168.1 eV, corresponding to the C-SO_3^- peak.[18] Through quantification of these XP spectra, we observed that after annealing, the atomic percentage (at%) of S in PS1 decreased from 6.78 at% to 5.28 at%, in comparison to the at% of S in MoS_2. By integrating the area of the C-SO_3^- peak in the S 2p spectra, we determined the presence of sp^2 carbon in the C 1s spectra, as shown in **Figure S9 c and g**, with a binding energy of 284.5 eV. The sp^3 carbon, C=O and O-C=O components were attributed to contamination. Additionally, the C-O/C-S peak at 286.5 eV partially originated from contamination and the C-S bond in PS1.[19]

We deconvoluted the O 1s peak, at a binding energy of 532.3 eV, into three components: Mo-O component (derived from the MoO_3 doublets integral in the Mo 3d spectra), O-S component (obtained from the C-SO_3^- doublets integral in the S 2p spectra), and O-C component (resulting from the contamination carbon integral in the C 1s spectra), which share the same peak position and FWHM, as shown in **Figure S9 d and h**. We observed that the ratio of S-O peak to Mo-O peak decreased after annealing the MoS_2 film at 150 °C for 180 min, while the ratio of MoO_3 to MoS_2 in the Mo 3d spectra remained constant before and after annealing. This decrease in the S-O peak indicated that some PS1 molecules have been removed after annealing. Based on our quantification XP spectra on all components, we determined that the content of PS1 molecules in the MoS_2 film slightly decreased from 1.58 at% to 1.38 at% following annealing at 150 °C for 180 min.

Figure S9. XPS spectra of annealed MoS_2 and pristine MoS_2 film drop-casted on SiO_2/Si substrate. (a-d) Pristine MoS_2 film. (e-h) Annealed MoS_2 film. Annealing was performed at 150 °C for 180 min.

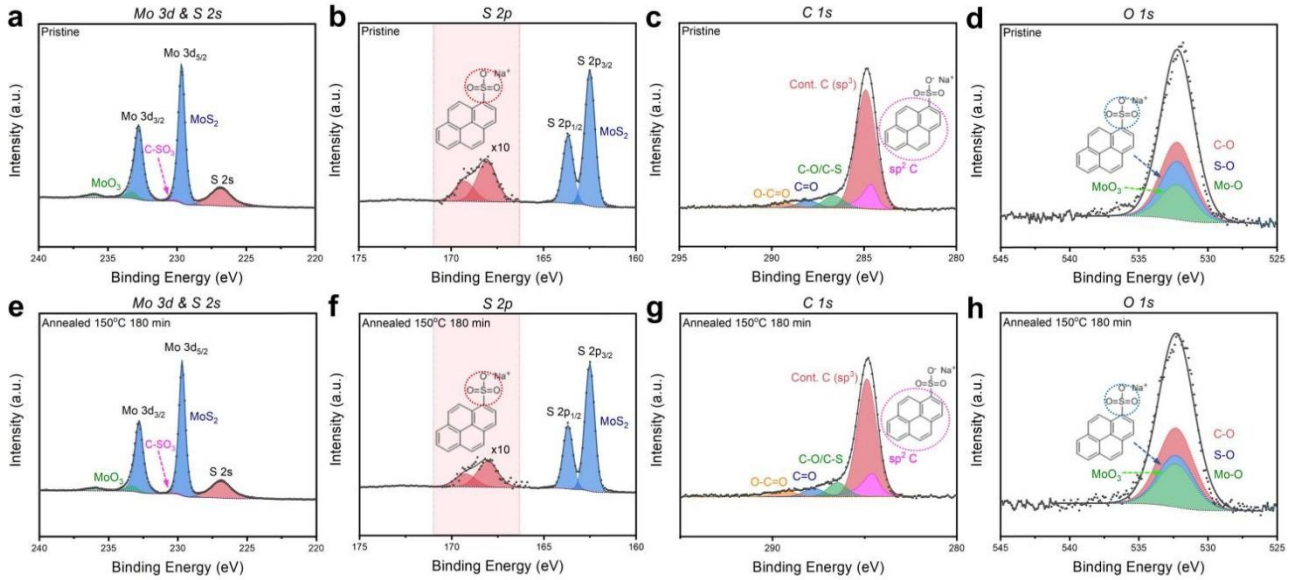

Supplementary Table IV. Constraints used for fitting XPS spectra in annealed and pristine MoS_2 film.

Components	Species	Line shape	Peak Position Constraints (eV)	Area Constraints	FWHM (eV) & Constraints
Mo 3d and S 2s					
A	S-Mo S 2s	GL(30)	B - 2.80	/	1.9 ± 0.1
B	Mo^{4+}-S Mo $3d_{5/2}$	GL(80)	229.70 ± 0.10	/	0.6 ± 0.1
C	C-SO_3^- S 2s	GL(30)	B + 0.71	A * 0.058	A * 1
D	Mo^{4+}-S Mo $3d_{3/2}$	GL(80)	B + 3.10	B * 0.67	B * 1.3
E	Mo^{6+}-O Mo $3d_{5/2}$	GL(80)	B + 3.62	/	1.2 ± 0.1
F	Mo^{6+}-O Mo $3d_{3/2}$	GL(80)	B + 6.36	D * 0.67	D * 1
S 2p					
A	Mo-S S $2p_{3/2}$	GL(30)	162.50 ± 0.10	/	0.61 ± 0.1
B	Mo-S S $2p_{1/2}$	GL(30)	A + 1.18	A * 0.5	A * 1
C	C-SO_3^- S $2p_{3/2}$	GL(30)	A + 5.54	/	1.30 ± 0.1
D	C-SO_3^- S $2p_{1/2}$	GL(30)	A + 6.72	C * 0.5	C * 1
C 1s					
A	sp^2 C	LA(1.2,2.5,5)	284.49 ± 0.10	derived from C-SO_3^- S 2p	0.80 ± 0.1
B	Cont C	GL(30)	A + 0.30	/	1.2 ± 0.1
C	C-O/C-S	GL(30)	A + 1.89	/	B * 1
D	C=O	GL(30)	A + 3.18	/	B * 1
E	O-C=O	GL(30)	A + 4.75	/	B * 1
O 1s					
A	O-C	GL(30)	532.3 ± 0.1	derived from C-O/C=O/O-C=O C 1s	3.04 ± 0.1
B	Mo-O	GL(30)	A + 0	derived from Mo^{6+}-O Mo 3d	A * 1
C	S-O	GL(30)	A + 0	derived from C-SO_3^- S 2p	A * 1

S5 Additional electrical measurements on Ag/MoS_2/Gr memristors

Figure S10. The current response from input voltage pulses generated by the Ag/MoS_2/Gr device.

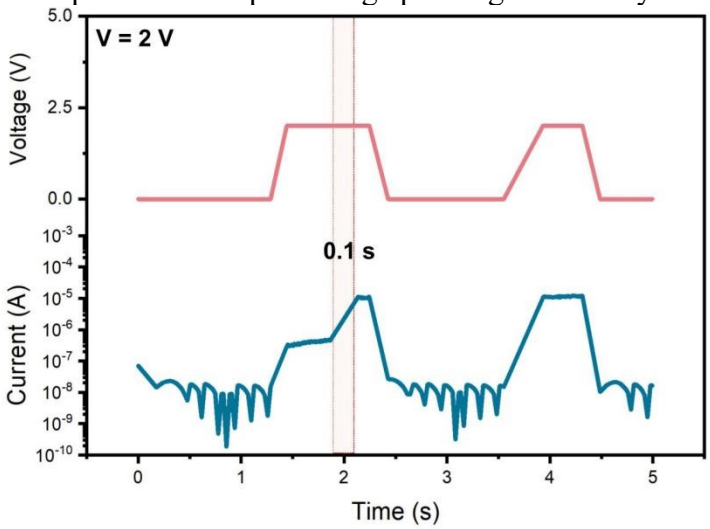

Figure S11. (a) Cycle endurance of a single Ag/MoS_2/Gr, set/reset by 4 V/-4 V and read by 0.5 V. (b) Data retention at LRS and HRS measured by I–t sampling, read at 0.1 V every 10 seconds and the time duration for 10000 seconds. (c) Data retention at LRS measured by I–t sampling, read at 1×10^{-5} V every 50 ms and the time duration for 80 seconds.

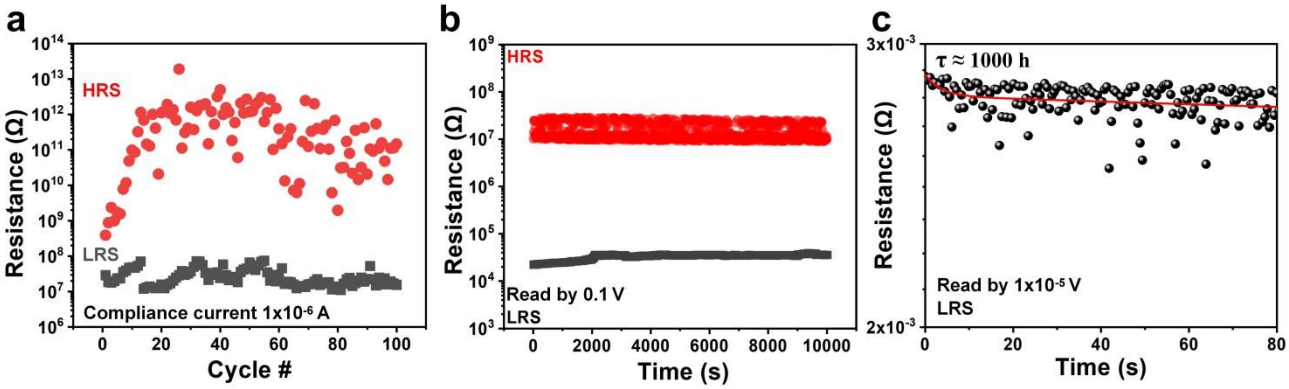

Figure S12. The current response from input voltage pulses generated by the Ag/MoS_2/Gr device, (a) Pulse voltage: 3V, time: 3.2 s. (b) Pulse voltage: 2V, time: 3.2 s. (c) Pulse voltage: 3V, time: 0.5 s. (d) Pulse voltage: 3V, time: 0.6 s.

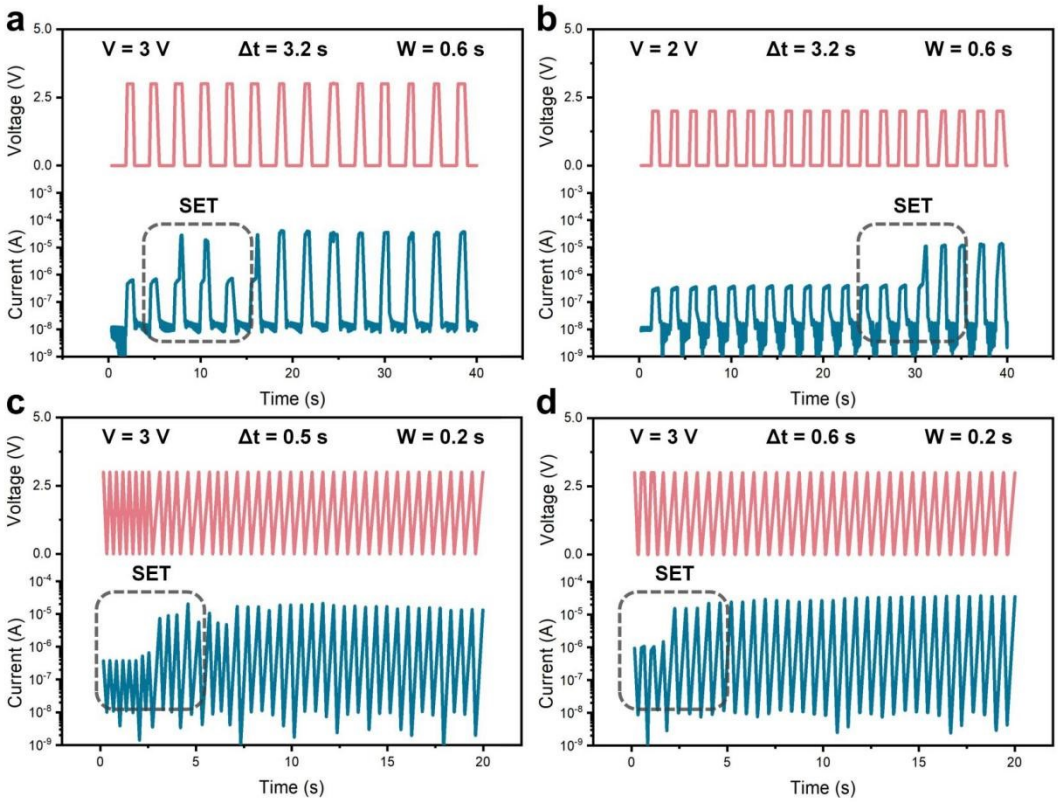

Figure S13. Cycle endurance of the Ag/MoS_2/Gr device with a set voltage of 3V.

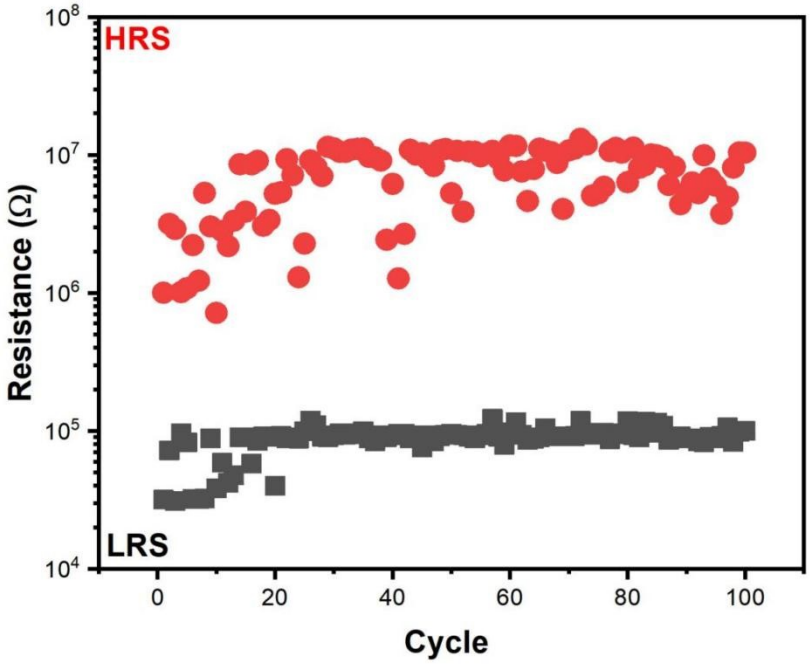

S6. Fully printed Ag/MoS_2/Gr memristors on Kapton

Figure S14. Resistive switching characteristics of Ag/MoS_2/Gr memristor on Kapton.

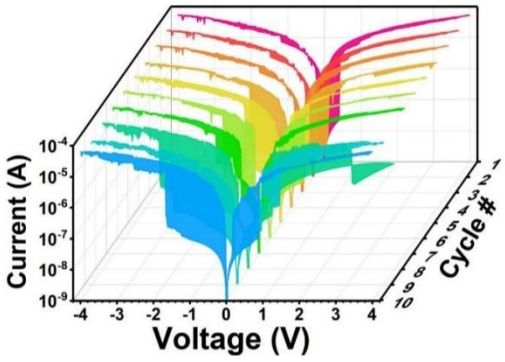

Figure S15. Cycle endurance of a single Ag/MoS_2/Gr on Kapton. (a) Pristine device. (b) 1% strain device, bending radius 2.5 mm. (c) 2% strain device, bending radius 1.25 mm.

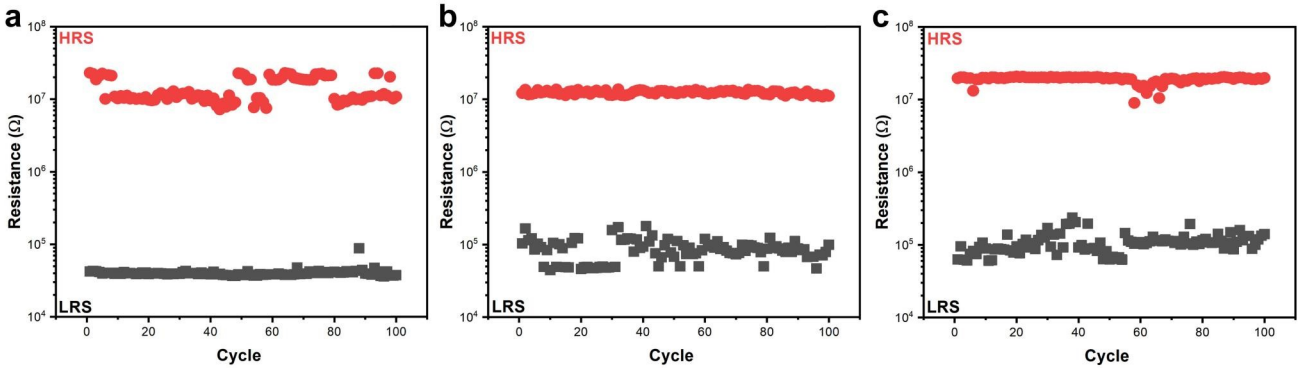

Figure S16. Bending endurance of a Ag/MoS_2/Gr device printed on Kapton. (a) LRS and HRS (b) I-V characteristics measured over 500 bending time (bending radius of 2.5 mm, corresponding to 1% strain). (c) LRS and HRS (d) I-V characteristics measured over 500 bending time (bending radius of 1.25 mm, corresponding to 2% strain).

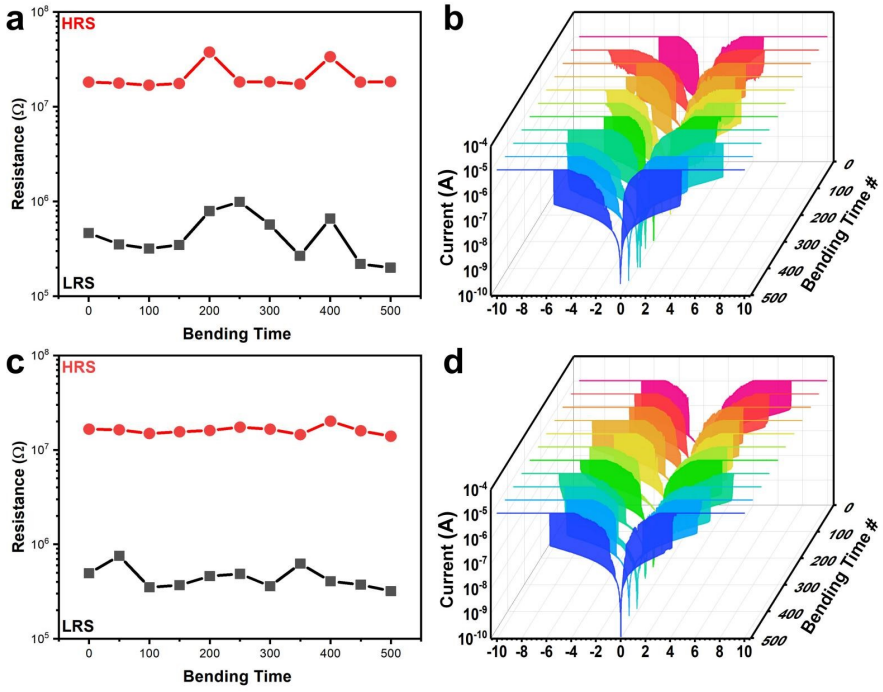

Supplementary Table V. Summary of switching voltage of the 10 Ag/MoS_2/Gr devices on Kapton under bending conditions.

Number of samples	Switching voltage (Strain 0%)	Switching voltage (Strain 1%)	Switching voltage (Strain 2%)	Switching voltage (Strain 3%)
Device 1	3.25 V	2.46 V	3.62 V	16.34 V
Device 2	1.32 V	1.76 V	3.04 V	8.42 V
Device 3	2.10 V	2.32 V	4.28 V	17.22 V
Device 4	1.74 V	3.12 V	3.00 V	3.55 V
Device 5	2.18 V	3.04 V	3.36 V	3.15 V
Device 6	1.84 V	3.38 V	3.72 V	1.12 V
Device 7	2.66 V	1.56 V	1.98 V	1.26 V
Device 8	2.22 V	3.88 V	1.91 V	2.06 V
Device 9	3.94 V	3.01 V	4.30 V	2.70 V
Device 10	1.74 V	5.65 V	5.88 V	10.66 V

S7. Fully printed Gr/MoS_2/Gr memristors on silicon

Figure S17. I-V curves for Gr/MoS_2/Gr devices.

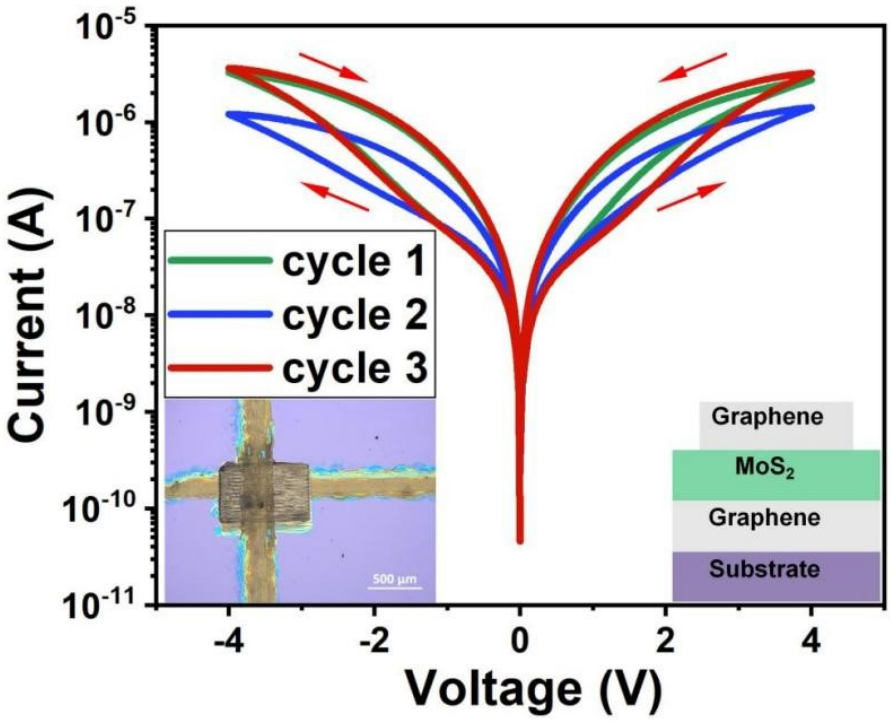

S8. Calculation of the filament temperature

For this set of measurements **(Figure S18)**, we applied a voltage with a constant amplitude (V, which was set to 1 V, 2 V, 5 V, 10 V, 15 V, 20 V, 25 V, 30 V, 40 V and 50 V during different tests) aimed to modify the conductance of the Ag/MoS_2/Gr devices. The duration of the voltage pulse and relaxation was 2 s. For each value of voltage pulse, reading current shows certain variability, but the overall increasing trend of current with voltage is very well fitted by an exponential function (**Figure S18 a**).

In **Figure S18 b**, *dI/dt* increases by the setting voltage, approximately exponentially at the beginning and rapidly when voltage reach 40 V, fingerprint of the formation of the conductive filament. As the physical meaning of f_1 is the power lost at the constriction, when setting voltage reach 40 V, f_1 should be close to 1, in agreement with large energy loss for the carriers passing through conductive filaments. As the voltage decreases, the f_1 will exponentially decrease to zero when the voltage reaches 0 V. This can be explained by considering that, as the anode-cathode voltage drop decreases, the number of channels available where energy loss can occur is also expected to decrease, and when the voltage drops to 0 V, the electrons at the cathode and at the anode will have the same energy, so no electron energy loss can occur, therefore, the percentage of electron energy loss should be zero.[20]

Figure S18. (a) The post-SET current for each pulse transient as a function of the pulse amplitude. (b) *dI/dt* data as a function of the setting voltage. f_1 parameter as a function of the setting voltage.

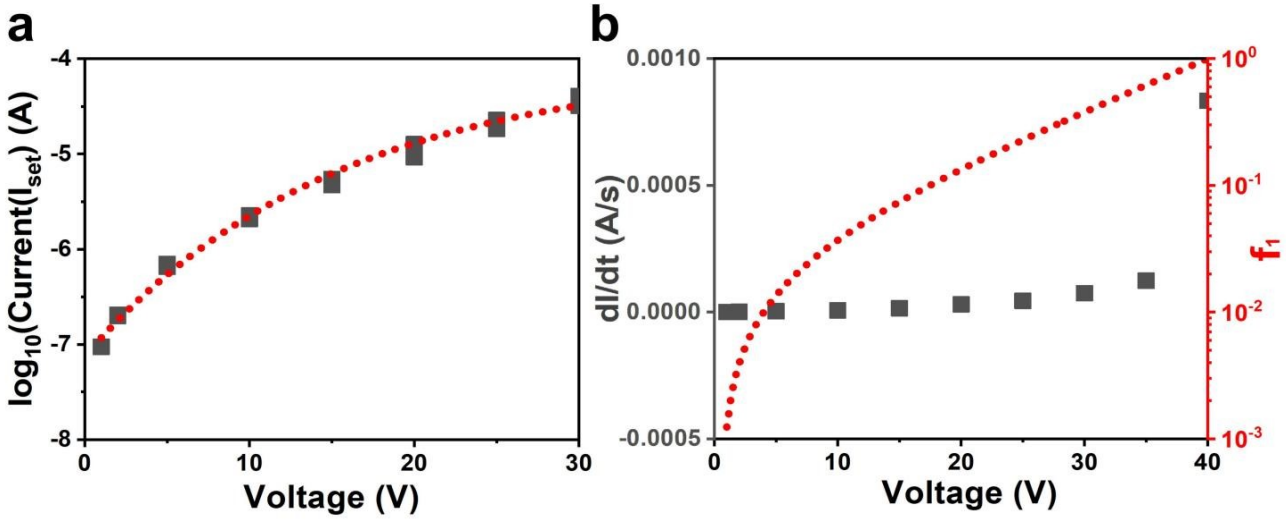

S9. Temperature dependence I-V measurements

Figure S19. I-V characteristics of the Ag/MoS_2/Gr memristors, (a) increasing temperature from 200 to 400 K, (b) decreasing temperature from 290 to 230 K, after formation switching.

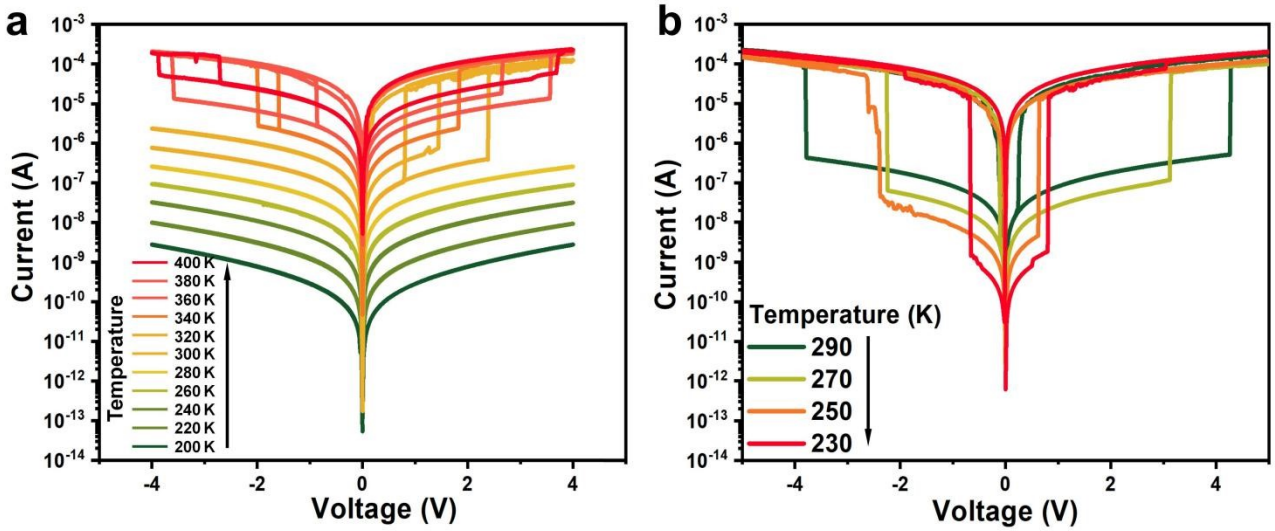

Supplementary Table VI. Summary of temperature dependent setting voltage in different devices.

Number of samples	Memristic appears	Device structure	Setting voltage
Device 1	260K-360K	Ag/MoS_2/Gr	1V-3.6V
Device 2	300K-400K	Ag/MoS_2/Gr	0.8 V-3.7 V

S10. Integration of CVD graphene

Figure S20 a and b show the optical image and the Raman spectrum of the CVD graphene transferred onto the SiO_2/Si substrate. The spectrum shows the characteristic G peak at 1580 cm^{-1},[21] while the D peak is not visible, hence confirming that the transfer process used does not damage the CVD graphene. **Figure S20 c and d** shows the optical pictures of the CVD graphene transferred onto the silver electrode and onto the MoS_2 layer. Table 4 shows a summary of the devices tested.

Devices are made with STS annealing. After the first annealing, the printability on the silicon is not good enough, so the sample is subjected to a 15 s Ar plasma treatment before the next material is printed. This treatment does not affect the structure of the printed MoS_2 film as shown by UV-Vis and Raman spectroscopy, **Figure S21 and S22**.

Figure S20. (a) Optical image of CVD graphene transferred on SiO_2/Si substrate. (b) Raman spectrum of CVD graphene on SiO_2/Si substrate. (c,d) Optical image of CVD graphene transferred on Ag electrode and onto the MoS_2 printed film.

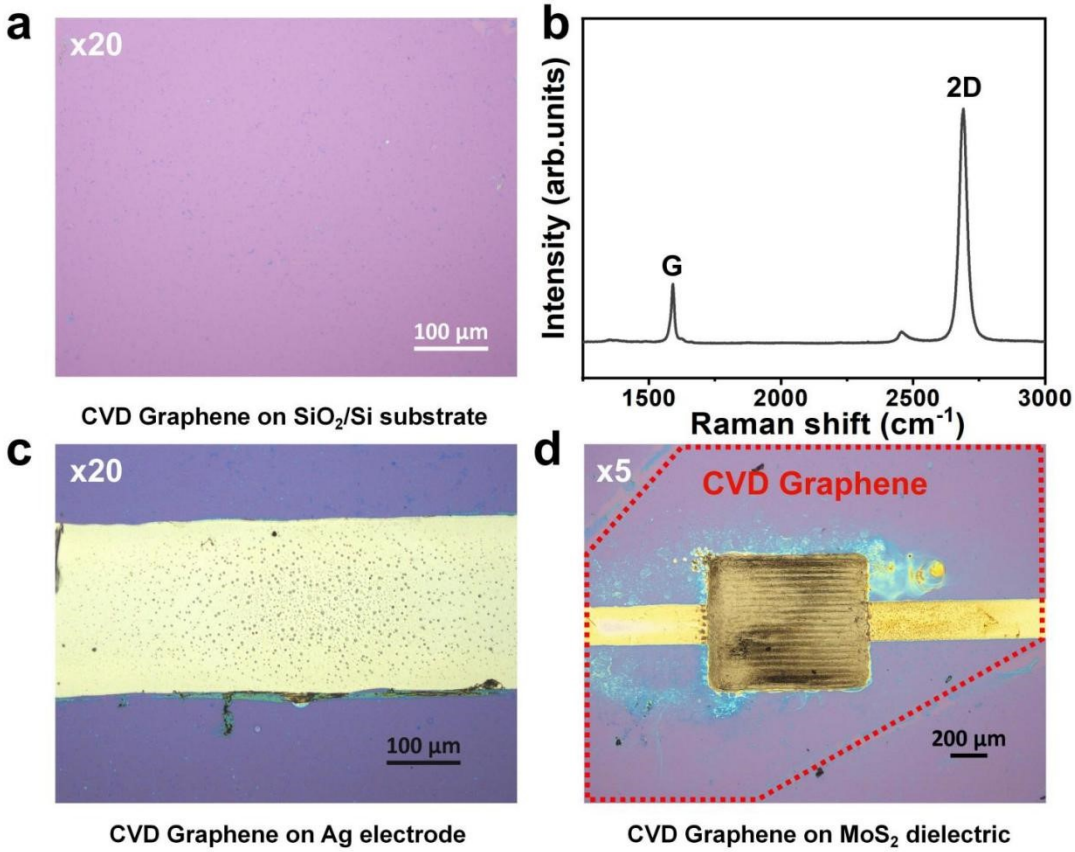

Figure S21. UV-vis absorption spectrum of pristine, annealed and plasma treated MoS_2 film.

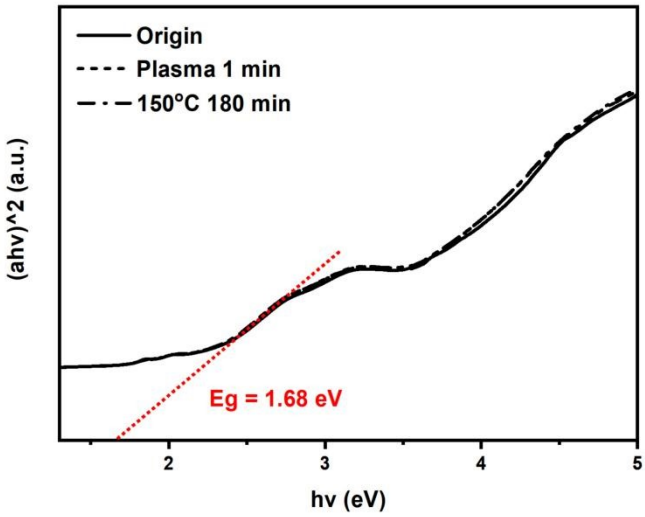

Figure S22. (a) Raman spectra of 80 print passes MoS_2 film before and after plasma treatment. (b) Raman spectra of 80 print passes MoS_2 film before and after annealing.

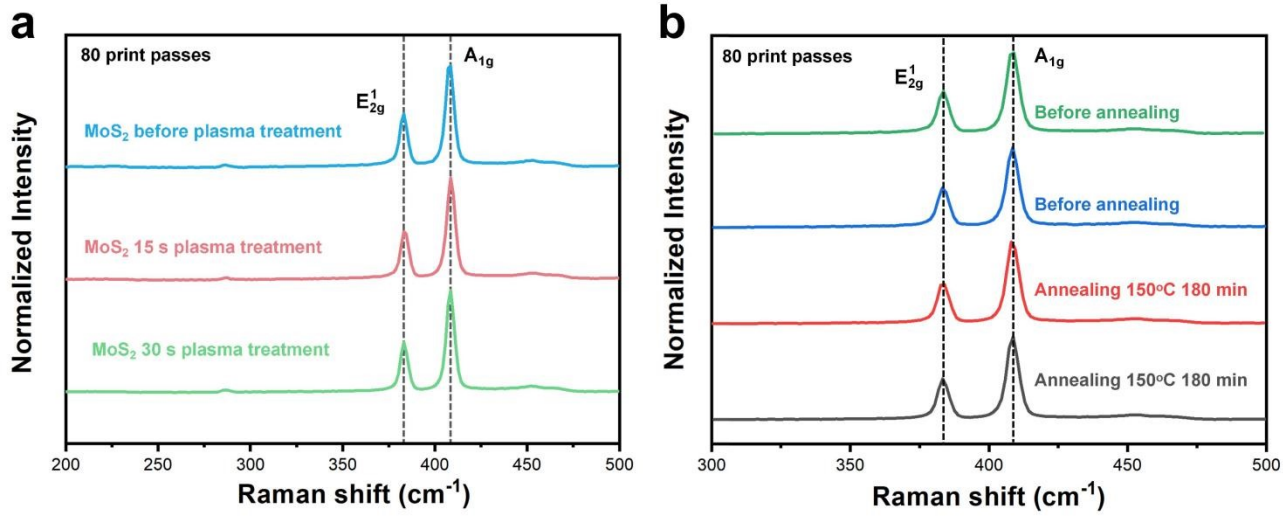

Figure S23. Resistive switching characteristics of all tested Ag/CVD Gr/MoS_2/Gr devices, tested over 3 cycles.

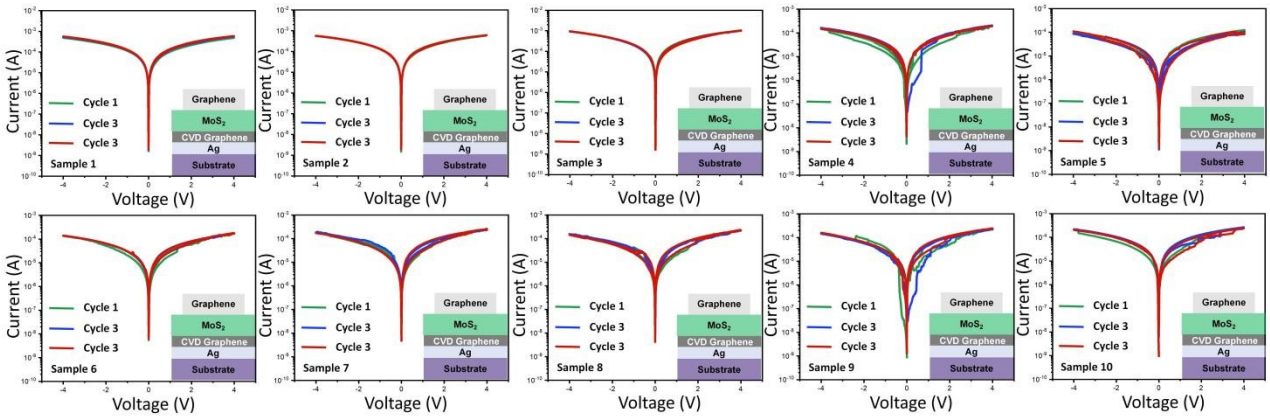

Figure S24. Resistive switching characteristics of all tested Ag/MoS_2/CVD Gr/Gr devices, tested over 3 cycles.

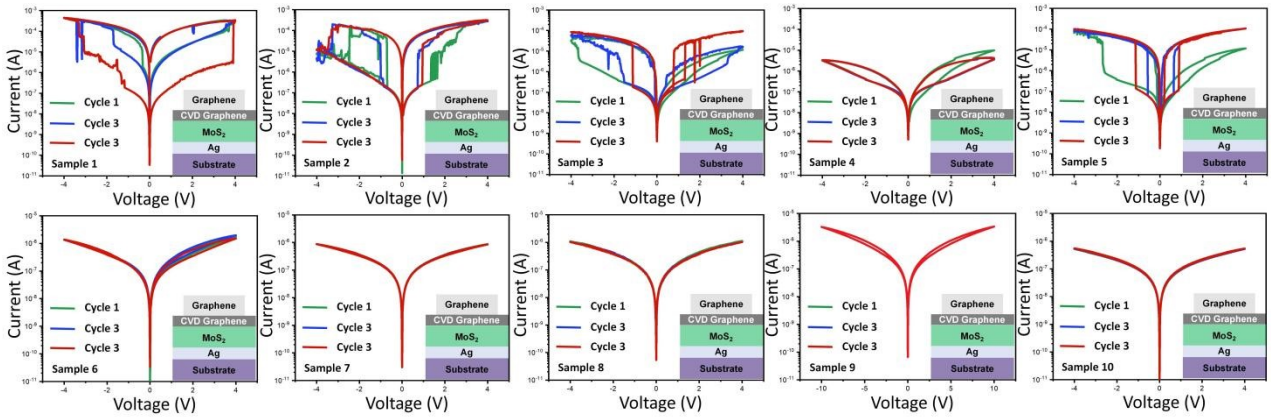

Figure S25. Resistive switching characteristics of all tested Ag/MoS_2/CVD Gr/MoS_2/Gr devices, tested over 3 cycles.

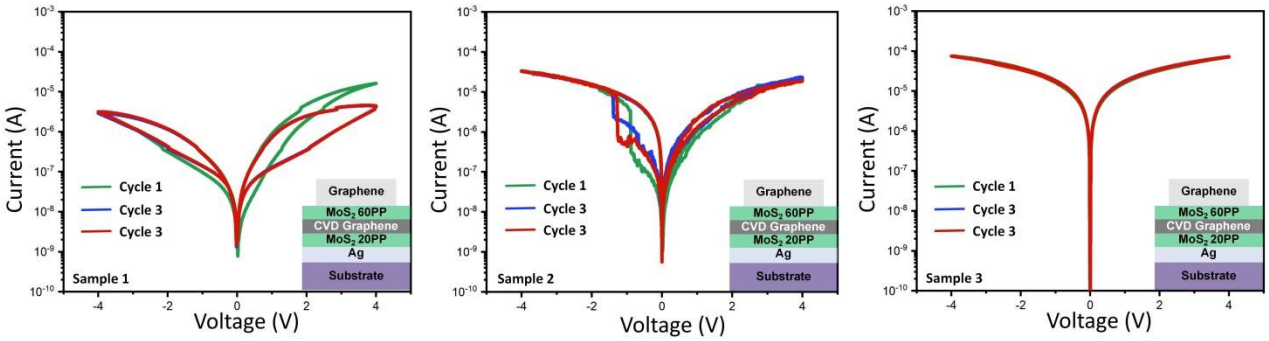

Supplementary Table VII. Summary of different-structure devices and memristic behavior.

Number of samples	Annealing	Device structure	Memristic/Hysteresis behavior
Over 50	STS	Ag/MoS_2/Gr	Memristic behavior
Over 50	FS	Ag/MoS_2/Gr	Memristic behavior
5	STS	Gr/MoS_2/Gr	Hysteresis behavior
10	STS before CVD Gr	Ag/MoS_2/CVD Gr/Gr	Memristic behavior (5 device) No Hysteresis (5 device)
3	STS before CVD Gr	Ag/MoS_2/CVD Gr/MoS_2/ Gr	Hysteresis behavior
10	STS before CVD Gr	Ag/CVD Gr/MoS_2/Gr	No Hysteresis

References

[1] K. H. Choi, M. Mustafa, K. Rahman, B. K. Jeong, Y. H. Doh, *Appl. Phys. A* **2012**, *106*, 165.

[2] N. M. Muhammad, N. Duraisamy, K. Rahman, H. W. Dang, J. Jo, K. Y. Choi, *Curr. Appl. Phys.* **2013**, *13*, 90.

[3] N. Duraisamy, N. M. Muhammad, H. Kim, J. Jo, K. Choi, *Thin Solid Films* **2012**, *520*, 5070.

[4] G. Siddiqui, J. Ali, Y. Doh, K. H. Choi, *Mater. Lett.* **2016**, *166*, 311.

[5] M. J. Catenacci, P. F. Flowers, C. Cao, J. B. Andrews, A. D. Franklin, B. J. Wiley, *J. Electron. Mater.* **2017**, *46*, 4596.

[6] B. Salonikidou, A. Mehonic, Y. Takeda, S. Tokito, J. England, R. A. Sporea, *Adv. Eng. Mater.* **2022**, *24*, 2200439.

[7] A. F. Rafique, J. H. Zaini, M. Z. Bin Esa, M. M. Nauman, *Appl. Phys. A*, **2020**, *126*, 134.

[8] M. M. Nauman, M. Z. Esa, J. H. Zaini, A. Iqbal, S. Abu Bakar, in *2020 IEEE 11th International Conference on Mechanical and Intelligent Manufacturing Technologies (ICMIMT)*, Cape Town, South Africa, **2020**, 167.

[9] K. Zhu, G. Vescio, S. González-Torres, J. López-Vidrier, J. L. Frieiro, S. Pazos, X. Jing, X. Gao, S. D. Wang, J. Ascorbe-Muruzábal, J. A. Ruiz-Fuentes, A. Cirera, B. Garrido, M. Lanza, *Nanoscale* **2023**, *15*, 9985.

[10] X. Feng, Y. Li, L. Wang, S. Chen, Z. G. Yu, W. C. Tan, N. Macadam, G. Hu, L. Huang, L. Chen, X. Gong, D. Chi, T. Hasan, A. V. Thean, Y. Zhang, K. Ang, *Adv. Electron. Mater.* **2019**, *5*, 1900740.

[11] Y. Li, X. Feng, M. Sivan, J. F. Leong, B. Tang, X. Wang, J. N. Tey, J. Wei, K. W. Ang, A. V. Y. Thean, *IEEE Sens. J.* **2020**, *20*, 4653.

[12] D. Lien, Z. Kao, T. Huang, Y. Liao, S. Lee, J. He, *ACS Nano* **2014**, *8*, 7613.

[13] G. U. Siddiqui, M. M. Rehman, K. H. Choi, *Polymer* **2016**, *100*, 102.

[14] M. N. Awais, H. C. Kim, Y. H. Doh, K. H. Choi, *Thin Solid Films* **2013**, *536*, 308.

[15] M. Khan, H. M. M. U. Rehman, R. Tehreem R, M. Saqib, M. M. Rehman, W. Y. Kim, Nanomaterials **2022**, *12*, 2289.

[16] J. C. Wildervanck, F. Jellinek, *Z Anorg Allg Chem* **1964**, *328*, 309.

[17] M. A. Baker, R. Gilmore, C. Lenardi, W. Gissler, *Appl. Surf. Sci.* **1999***, 150,* 255.

[18] P. Gobbo, M. C. Biesinger, M. S. Workentin, *Chem. Commun.* **2013**, *49*, 2831.

[19] M. C. Biesinger, *Appl. Surf. Sci.* **2022**, *597*, 153681.

[20] S. Lombardo, E. Y. Wu, J. H. Stathis, *J. Appl. Phys.* **2017**, *122*, 085701.

[21] A. C. Ferrari, J. C. Meyer, V. Scardaci, C. Casiraghi, M. Lazzeri, F. Mauri, S. Piscanec, D. Jiang, K. S. Novoselov, S. Roth, A. K. Geim, *Phys. Rev. Lett.* **2006**, *97*, 187401.